Article:
Hunt, Neil Terrence (2019) Uncovering the Early Stages of Domain Melting in Calmodulin With Ultrafast Temperature-Jump Infrared Spectroscopy. Journal of Physical Chemistry B. ISSN: 1520-5207

https://doi.org/10.1021/acs.jpcb.9b08870

THE JOURNAL OF PHYSICAL CHEMISTRY B

Article

Cite This: J. Phys. Chem. B XXXX, XXX, XXX−XXX

pubs.acs.org/JPCB

Uncovering the Early Stages of Domain Melting in Calmodulin with Ultrafast Temperature-Jump Infrared Spectroscopy

Lucy Minnes,[†] Gregory M. Greetham,[‡] Daniel J. Shaw,[§] Ian P. Clark,[‡] Robby Fritzsch,[†] Michael Towrie,[‡] Anthony W. Parker,[‡] Alistair J. Henry,[§] Richard J. Taylor,[§] and Neil T. Hunt*[,∥]

[†]Department of Physics, SUPA, University of Strathclyde, Glasgow G4 0NG, United Kingdom

[‡]STFC Central Laser Facility, Research Complex at Harwell, Rutherford Appleton Laboratory, Harwell Campus, Didcot OX11 0QX, United Kingdom

[§]UCB Pharma, Slough SL1 3WE, United Kingdom

[∥]Department of Chemistry and York Biomedical Research Institute, University of York, Heslington, York YO10 5DD, United Kingdom

Supporting Information

ABSTRACT: The signaling protein calmodulin (CaM) undergoes a well-known change in secondary structure upon binding Ca^{2+}, but the structural plasticity of the Ca^{2+}-free *apo* state is linked to CaM functionality. Variable temperature studies of *apo*-CaM indicate two structural transitions at 46 and 58 °C that are assigned to melting of the C- and N-terminal domains, respectively, but the molecular mechanism of domain unfolding is unknown. We report temperature-jump time-resolved infrared (IR) spectroscopy experiments designed to target the first steps in the C-terminal domain melting transition of human *apo*-CaM. A comparison of the nonequilibrium relaxation of *apo*-CaM with the more thermodynamically stable *holo*-CaM, with 4 equiv of Ca^{2+} bound, shows that domain melting of *apo*-CaM begins on microsecond time scales with α-helix destabilization. These observations enable the assignment of previously reported dynamics of CaM on hundreds of microsecond time scales to thermally activated melting, producing a complete mechanism for thermal unfolding of CaM.

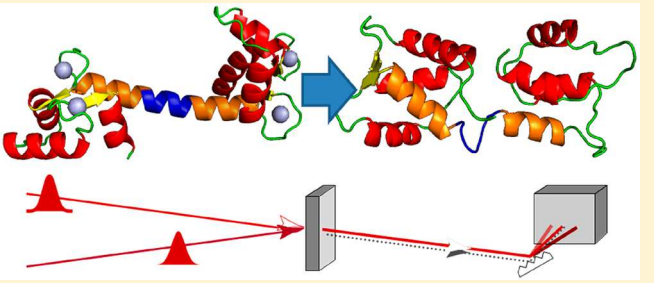

INTRODUCTION

The link between structure and function in biological molecules is well-established and raises important questions given that proteins are dynamic in the solution phase. This means that having the ability to follow the mechanisms of structural change in real time is imperative if we are to understand and modify protein behavior *in vivo*. Observing protein structural transitions is technologically challenging, however, due to the complexity of the associated macromolecular potential energy surfaces, which are multidimensional in terms of both degrees of structural freedom and the range of time scales over which transitions occur.

Temperature-jump (T-jump) initiation offers a powerful approach to understanding biomolecular dynamics.[1−4] T-jump pump−probe methodology exploits infrared wavelength excitation of water to create a fast rise in temperature in an aqueous biomolecular system, followed by a time delayed probe of the evolving system. The probe method employed to study proteins or peptides includes fluorescence,[5] circular dichroism,[6] and infrared spectroscopy.[3] The latter is particularly attractive because of the sensitivity of the amide I vibrational mode of the peptide backbone link to protein secondary structure and local molecular environment.

T-jump methods have been used to access time scales ranging from the nanosecond pulse duration of the excitation laser to the milliseconds required for the temperature-jump to dissipate.[1−4,6−16] An alternative strategy employed solvated dyes to achieve a rapid temperature change,[17] while jumps in pH have also been used to study peptide structural transitions.[18] An advantage in using temperature or pH to perturb proteins is the ability to explore their potential energy surface in the absence of structural modifications or non-natural entities.[19−22]

In the case of protein or peptide systems, T-jump IR methods have largely been applied to short chain peptides, where unfolding time scales are on the order of a few microseconds for typical α-helical and β-turn systems.[1−3,23] More recently, T-jumps combined with vibrational echo probing have been applied to study processes involving larger proteins, including ubiquitin unfolding and insulin dimer formation.[8,11,13,24] It was reported that protein unfolding occurs on two time scales. Hundreds of microsecond dynamics were assigned to the crossing of energetic barriers in response to the elevated

Received: September 18, 2019
Revised: September 26, 2019
Published: September 26, 2019

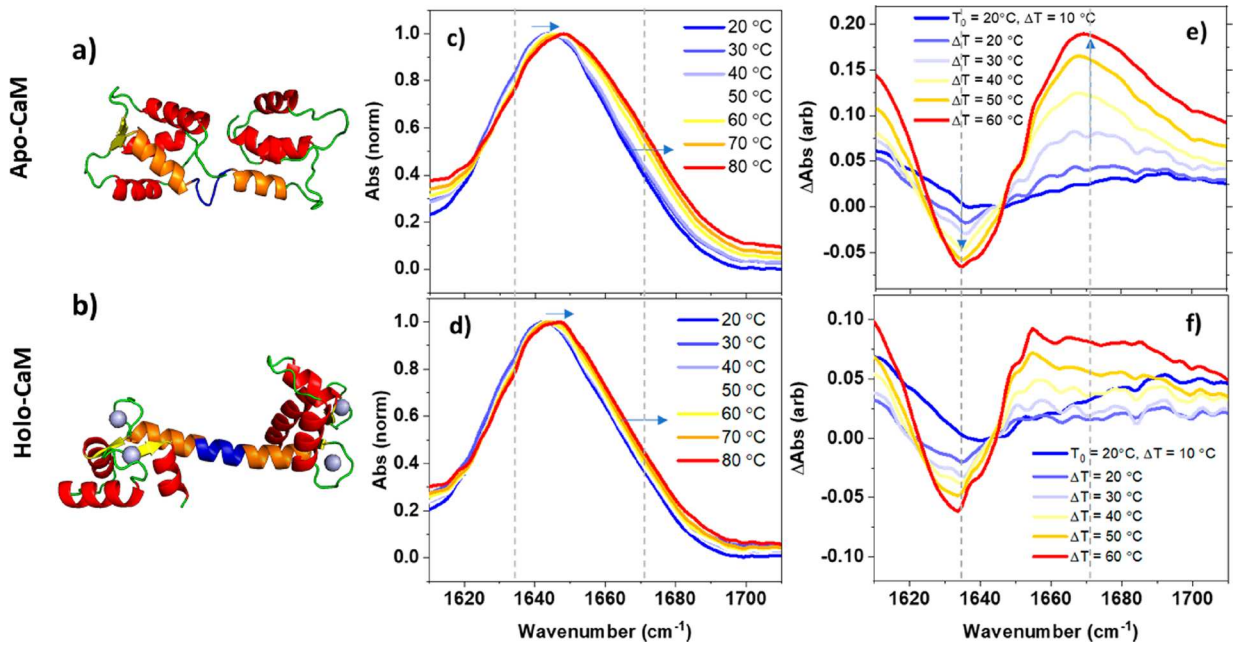

Figure 1. Structures of (a) *apo*-CaM and (b) *holo*-CaM showing α-helices (red), β-strands (yellow), flexible central linker (orange and blue), and Ca^{2+} ions (gray). (c, d) IR absorption spectra of *apo*-CaM (c) and *holo*-CaM (d) as a function of temperature. (e, f) Difference IR absorption spectra of *apo*-CaM (e) and *holo*-CaM (f) as a function of temperature relative to the spectrum obtained at 20 °C. The spectra are labeled using the convention of T_0, which indicates the starting temperature of the solution, and ΔT, which indicates the size of the temperature increase.

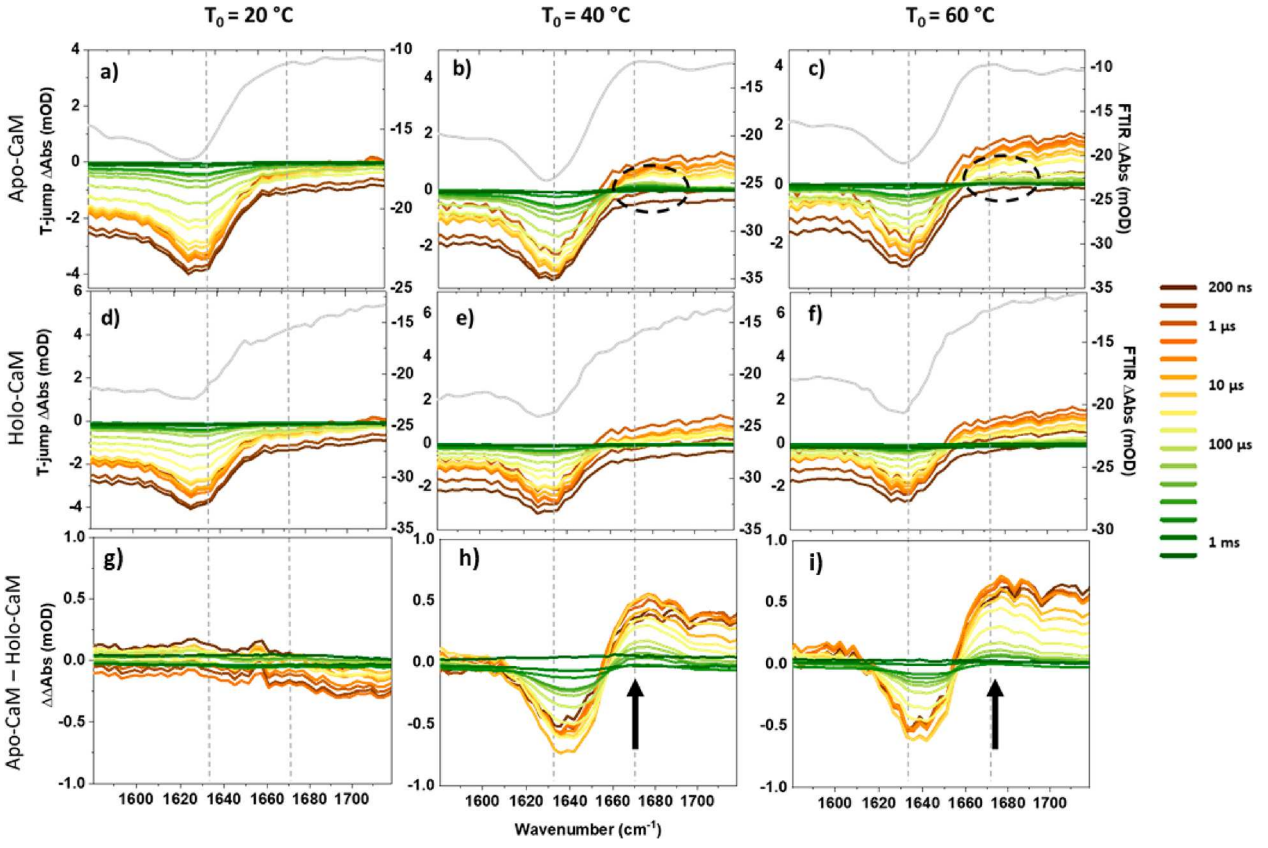

Figure 2. T-jump pump-IR probe spectra for *apo*-CaM (a–c) and *holo*-CaM (d–f). Data are shown for three representative values of T_0: 20, 40, and 60 °C in the left, center, and right columns, respectively. Gray spectra show IR absorption difference spectra corresponding to a rise in temperature of 9 °C from T_0 for comparison. (g–i) Double difference spectra showing $[S_{apo} - S_{holo}]$ T-jump data for each value of T_0 and T-jump pump-IR probe delay time (τ_{pp}).

temperature, but rapid unfolding processes taking just a few microseconds were also observed and attributed to downhill unfolding, constituting the first steps of the structural rearrangement.[11]

DOI: 10.1021/acs.jpcb.9b08870
J. Phys. Chem. B XXXX, XXX, XXX–XXX

We report the use of high pulse repetition rate T-jump pump-IR probe spectroscopy[25] to target the fastest steps in the unfolding of the human calmodulin protein (CaM). CaM is a multifunctional calcium-binding messenger protein found in many eukaryotic cells. At room temperature in solution, the CaM structure is largely conserved across a range of organisms,[26−29] consisting of α-helical sections organized into two (C- and N-terminal) globular domains, each containing helix−loop−helix E-F hand motifs (Figure 1a,b, red). Each domain houses a pair of Ca^{2+} ion binding sites. In the absence of Ca^{2+} the two domains are connected by a central linker, which features two α-helices (Figure 1a, orange) joined by a short random coil (Figure 1a, blue). Upon uptake of four Ca^{2+} ions, the random coil element becomes helical leading to the fully extended *holo*-CaM structure (Figure 1b).[30,31] While the *apo*−*holo* structural transition is well-understood,[29,32−44] the presence of significant structural plasticity in both states[31,35,45−48] is believed to contribute to CaM function *in vivo*.[49−53]

The application of T-jump methods to CaM will shed important new light on the stability of the structure and the mechanism of unfolding. Recently, we demonstrated that ultrafast IR spectroscopy provides a sensitive probe of the structural changes occurring in CaM, using 2D-IR methods at a range of temperatures to probe the equilibrium structures of *apo*- and *holo*-CaM.[54] Our work showed that CaM exhibits temperature sensitive IR spectra in both *apo* and *holo* states and that the thermodynamically more stable *holo*-CaM can be used to provide a benchmark for changes in solvation of the protein that accompany heating without a structural transition. By contrast, the IR spectrum of *apo*-CaM contains contributions from both changes in solvation and domain melting. These results form the basis of this time-resolved study of CaM unfolding in which a 9 °C T-jump was used to observe *apo*-CaM domain melting, using *holo*-CaM as a reference. With a focus on time scales shorter than 100 μs, our results develop upon the single previous time-resolved study of CaM, which reported two-state unfolding of the C-terminal domain on several hundred microsecond time scales.[35]

RESULTS AND DISCUSSION

Infrared absorption spectra of *apo*- and *holo*-CaM show that the amide I band of both proteins shifts to a higher wavenumber upon heating (Figure 1c−f). Difference IR absorption spectra relative to the spectrum at 20 °C are shown in Figure 1e,f. In preparation for discussion of T-jump data below, these are labeled using the convention of T_0, to indicate the starting temperature of the solution, and ΔT, to indicate the size of the temperature increase. For T-jump measurements discussed below, ΔT will remain constant at 9 °C, while T_0 will vary.

The IR absorption difference spectra (Figure 1e) show that the amide I band of *apo*-CaM undergoes a decrease in intensity at 1636 cm^{-1} and a gain of intensity in a well-defined band centered at 1671 cm^{-1} (blue arrows and gray dashed lines).[54] In the case of *holo*-CaM (Figure 1f), a loss of intensity near 1635 cm^{-1} was accompanied by a broad and rather featureless gain in intensity peaking near 1658 cm^{-1} but extending toward 1700 cm^{-1}. These results have been assigned previously, with the aid of circular dichroism, differential scanning calorimetry (DSC), and 2D-IR spectroscopy, to the effects of increased temperature of the solvent combined, in the case of *apo*-CaM, with a helix-to-coil transition consistent with C-terminal domain melting at 46 °C.[54]

Representative T-jump pump-IR probe spectroscopy results are shown for *apo*-CaM (Figure 2a−c) and *holo*-CaM (Figure 2d−f) at T_0 values of 20, 40, and 60 °C. The design and implementation of the spectrometer were reported recently.[25] The temporal profile of the T-jump was calibrated using the asymmetric carboxylate stretching mode of trifluoroacetic acid (TFA) solutions (see SI Figures S1−S3),[25] revealing a 9 °C T-jump within the 4 ns pulse duration of the pump laser that relaxed in a manner well-described by a stretched exponential function

$$\Delta A = \alpha \exp\left(-\frac{\tau_{pp}}{\tau_1}\right)^{\beta}$$

with a lifetime of $\tau_1 \sim 47$ μs and β parameter of 0.54 (Figure 3, black). In the equation, ΔA indicates the measured change in absorbance, τ_{pp} the T-jump-probe delay time, and α the amplitude of the signal. The stretched exponential character originates largely from a heterogeneous temperature-jump distribution across the sample cell caused by absorption of the T-jump pulse by the OD stretching vibration.[25]

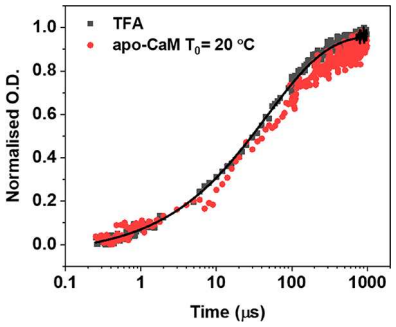

Figure 3. Temporal response of the T-jump as calibrated using a trifluoroacetic acid (TFA) solution (black), see text. This is compared to the results obtained for *apo*-CaM with a T_0 value of 20 °C (red). Results of fitting the temporal dynamics of the TFA T-jump data to a stretched exponential function (see text) are shown as a solid black line.

At T_0 = 20 °C, the T-jump-IR spectrum of the *apo*-CaM sample (Figure 2a) shows an instantaneous response consisting of a negative peak, indicating a decrease in absorbance, near 1635 cm^{-1} (gray dashed line). This is present from the shortest measured values of τ_{pp} (~1 ns) (Figure 2, dark red) and is superimposed upon a negative shift in the baseline of the difference spectrum that masks a small, almost flat, positive response to the high wavenumber side of the 1635 cm^{-1} peak. Both the baseline shift and the negative peak relax to zero intensity over a period of 1 ms (Figure 2, green) without any significant evolution in shape.

The response of the *apo*-CaM sample at T_0 = 20 °C is assigned to the result of the T-jump-induced perturbation. This is supported by comparison of the T-jump results with those from IR absorption spectroscopy (solid gray line, Figure 2a). Applying a ΔT of 9 °C to a sample with a T_0 of 20 °C gave an IR absorption difference profile that was almost identical in shape to the T-jump data. Furthermore, the relaxation dynamics of the T-jump spectral features in Figure 2a closely match those of the TFA calibration sample (Figure 3, red).

For *holo*-CaM at T_0 values of 20 °C, the response to the T-jump (Figure 2d) is almost identical to that of *apo*-CaM (Figure 2a). Raising the starting temperature of the sample to 40 °C leads to differences being observed between the *apo*- and *holo*-

DOI: 10.1021/acs.jpcb.9b08870
J. Phys. Chem. B XXXX, XXX, XXX−XXX

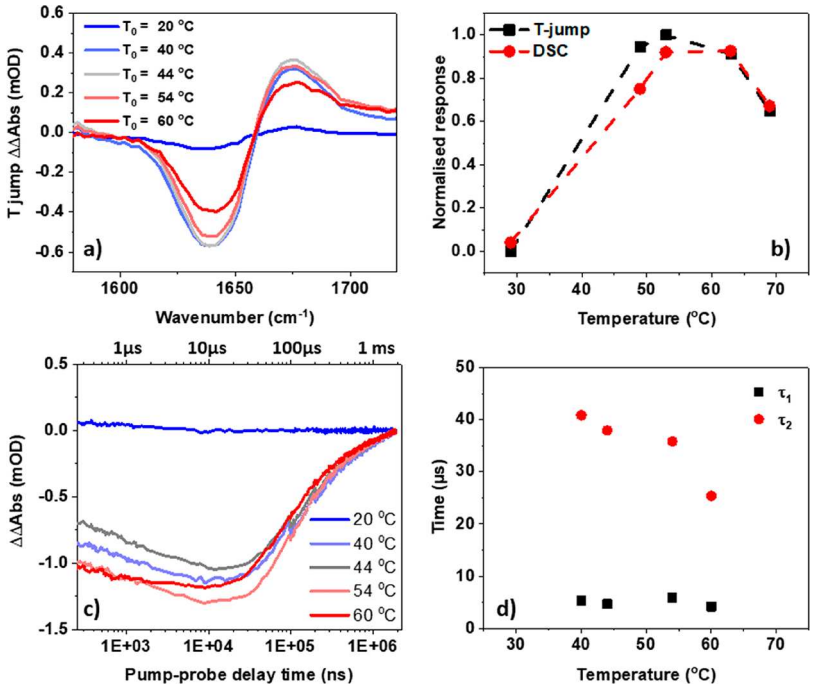

Figure 4. (a) Double difference $[S_{apo} - S_{holo}]$ T-jump spectra at a range of T_0 values for τ_{pp} = 100 μs. (b) Comparison of the amplitude of the T-jump double difference response shown in part a (black) with the results of DSC data obtained for *apo*-CaM (red).[54] The *y*-axis label "normalized response" refers to the magnitude of the T-jump double difference $[S_{apo} - S_{holo}]$ signal at 1640 cm^{-1} (as in part a) and C_p (μCal/°C) from DSC data. (c) Temporal dependence of the T-jump double difference response $[S_{apo} - S_{holo}]$ as a function of T_0. (d) Results of fitting the data in part c to a stretched biexponential function (see text).

CaM samples. While the *holo*-CaM data at T_0 = 40 °C (Figure 2e) closely resembled that at T_0 = 20 °C (Figure 2d), we observe the growth of a new spectral feature in the T_0 = 40 °C *apo*-CaM spectrum (Figure 2b, black dashed oval). This positive peak is most clearly visible in Figure 2b near 1670−1680 cm^{-1} at τ_{pp} values of ∼100 μs, before it relaxes to the baseline by τ_{pp} = 1 ms.

The results at a T_0 value of 60 °C for *apo*-CaM were similar to those at T_0 = 40 °C. Once again, an additional positive feature was present in the *apo*-CaM data (Figure 2c, black dashed oval), though this was smaller than that observed at T_0 = 40 °C, and the peak extended to a slightly higher wavenumber. By contrast, the T_0 = 60 °C *holo*-CaM spectra (Figure 2f) showed little variation from the T_0 = 20 °C result (Figure 2d).

To analyze the T-jump data in more detail, double difference spectra were created by subtracting the response of the *holo*-CaM sample from that of the *apo*-CaM sample, $[S_{apo} - S_{holo}]$, for given values of T_0 and τ_{pp}. This approach has twin benefits. First, the response of the solvent is expected to be similar in both cases, and so, its effect is removed from the T-jump data. Second, it has been demonstrated previously that the *holo*-CaM sample does not undergo a melting transition below 80 °C, and so the *holo*-CaM sample acts as a convenient reference for the impact of elevated solvent temperature on the protein amide I band.[54] Thus, any differences in the resultant double difference spectrum, $[S_{apo} - S_{holo}]$, can be confidently assigned to additional temperature-induced processes present in the former protein. The results are shown in Figure 2g−i, where the $[S_{apo} - S_{holo}]$ spectra are shown as a function of τ_{pp} for T_0 values of 20, 40, and 60 °C.

At T_0 = 20 °C, the $[S_{apo} - S_{holo}]$ spectrum shows that there is little variation in the responses of *apo*- and *holo*-CaM (Figure 2g) as would be expected given that the first structural transition occurs at 46 °C.[54] However, at T_0 = 40 °C (Figure 2h) it is clear that *apo*-CaM responds differently to the T-jump than the *holo*-CaM sample. The differences were characterized by fitting to Gaussian line shape functions, revealing negative and positive peaks at 1640 and 1671 cm^{-1}, respectively. These are present from early values of τ_{pp} (Figure 2h, dark red), indicating an effectively instantaneous response of *apo*-CaM to the increase in temperature of the solvent, but they subsequently grow in amplitude, peaking at τ_{pp} of ∼10 μs (Figure 2h, orange) before relaxing by τ_{pp} = 1 ms (Figure 2h, dark green). This is the same feature described in Figure 2b,c, but the spectral positions and temporal dependences are more clearly identified following the $[S_{apo} - S_{holo}]$ analysis.

Similar results were obtained at T_0 = 60 °C (Figure 2i), though the negative peak at 1640 cm^{-1} was smaller than that observed at T_0 = 40 °C, while the positive feature at 1675 cm^{-1} (black arrow) was broader with greater contributions at frequencies near 1700 cm^{-1}. Once again, the peak in the T-jump double difference spectra $[S_{apo} - S_{holo}]$ occurred at τ_{pp} ∼10 μs, with all features relaxing to the baseline by τ_{pp} = 1 ms.

Prior studies of the temperature dependence of the CaM IR spectrum have shown that melting of the C-terminal domain of CaM is accompanied by spectral density loss at 1636 cm^{-1} and a gain at 1671 cm^{-1}.[54] It is thus reasonable to conclude that the differences between the *apo*- and *holo*-CaM T-jump responses stem from domain melting in *apo*-CaM. This is further supported by examination of the amplitude of the $[S_{apo} - S_{holo}]$ double difference feature as a function of T_0. Figure 4a shows the T-jump double difference spectra obtained at τ_{pp} = 100 μs at a range of T_0 values. It can be seen that the spectral form of the response does not change dramatically with T_0, but the amplitude shows a strong correlation with a previously reported differential scanning calorimetry (DSC) temperature profile of *apo*-CaM (Figure 4b).[54] On this basis, the double

DOI: 10.1021/acs.jpcb.9b08870
J. Phys. Chem. B XXXX, XXX, XXX−XXX

difference spectral feature is assigned to a helix-to-coil process associated with melting of the C-terminal domain of *apo*-CaM induced by the 9 °C T-jump.

For T_0 = 54 and 60 °C, an increased amplitude was observed at higher wavenumber (~1700 cm^{-1}) in the $[S_{apo} - S_{holo}]$ spectrum (Figure 4a) and is tentatively assigned to the beginnings of the N-terminal domain melting process expected at 58 °C leading to a more unstructured *apo*-CaM protein and broader amide I signature.

Upon assignment of the T-jump spectra, it is instructive to consider the dynamics observed for the process. The temporal dependence of the $[S_{apo} - S_{holo}]$ double difference feature is shown in Figure 4c, which plots the magnitude of the α-helix feature near 1640 cm^{-1}; the results obtained for the peak-to-peak (1640−1671 cm^{-1}) magnitude were in close agreement. It can be seen that the peak is present from early values of τ_{pp}, reaches a maximum at around 10 μs, and relaxes by τ_{pp} = 1 ms. Fitting these dynamics to a stretched biexponential function (Figure S4) showed that the behavior is well-represented by a rising component with a time scale of ~5 μs and a decay of ~40 μs (Table 1 and Figure 4d). These time scales were largely

Table 1. Results of Fitting $[S_{apo} - S_{holo}]$ Dynamics to Stretched Double Exponential Function

T_0 (°C)	τ_1 (μs)	τ_2 (μs)	β_1	β_2
40	5.3	41	0.46	0.36
44	4.7	38	0.46	0.35
54	5.8	36	0.53	0.39
60	4.1	25	0.53	0.35

constant with T_0 (Figure 4d), though the longer time scale observed at T_0 = 60 °C was shorter, possibly due to the smaller amplitude of the melting process at an elevated temperature.

The longer time scale is very similar to that obtained in the TFA calibration experiments (47 μs) and is therefore assigned to the effects of cooling of the sample following the T-jump. In the current spectrometer configuration, the high T-jump pulse repetition rate (0.5 kHz, Supporting Information) provides more rapid data acquisition compared to lower repetition rate experiments, but it also requires the sample to have cooled by τ_{pp} = 2 ms in order to prevent gradual temperature buildup in the sample.[25] To avoid this, a short sample path length (6 μm) was employed, although one impact of this is that the excess temperature dissipates more rapidly than for longer path length samples. The result is that the spectrometer is optimized to observe the faster (<100 μs) melting dynamics, which complements techniques able to extend the visible window to tens of milliseconds.

The presence of a fast rising component in the $[S_{apo} - S_{holo}]$ signal shows that melting-related processes are occurring in the *apo*-CaM sample on ~5 μs time scales and that these are not present in the *holo*-CaM data (see also Figure 2). The time scales involved are comparable to previous observations of helical peptide melting and hairpin unfolding.[1−4] While such time scales may seem too fast for domain melting, we stress that the signals observed are small and the observations of these experiments represent the very fastest steps in a domain melting that does not go fully to completion. Justification for this can be found in the much greater magnitude of the IR absorption difference spectral signature, where equilibration at the new elevated temperature is achieved, relative to the T-jump difference spectra (Figures 1 and 2). Indeed, the time scales observed in the T-jump melting experiments are comparable with fast steps reported in the melting of ubiquitin, which were assigned to initial "burst phase" or downhill melting of the protein following T-jump perturbation of the potential energy surface for some of the proteins.[11] In those experiments, slower time scale dynamics on hundreds of microsecond time scales were assigned to activated barrier crossing caused by proteins re-equilibrating to the new temperature. In our current study, although the early processes are visible, sample cooling competes with any activated barrier crossing such that the results are dominated by the fast initial phase of the unfolding. This is supported by the lack of a T_0 dependence of the 5 μs unfolding time scale in all except for the T_0 = 20 °C data (where unfolding is not detected).

It is interesting to note that *apo*-CaM unfolding appears to begin with destabilization of α-helical components of the C-terminal domain. In a previous study, the results of molecular dynamics simulations were reported, which showed that the *apo*-CaM protein is significantly more flexible than its *holo* counterpart.[54] Indeed, the most flexible residues were reported to lie between positions 90 and 148 in the C-terminal domain. Although these were largely located in the coil sections between the helical parts of the C-terminal domain, it is reasonable to suggest, on the basis of prior studies of short chain peptides, that helix melting begins at the ends of the short helical sections, which link to the random coil units. Thus, the concept of domain unfolding beginning with fraying of the ends of helical sections would be consistent with both our results and other studies.[2,3]

CONCLUDING REMARKS

Comparison with the only other T-jump study of CaM unfolding shows a marked disparity in time scales.[35] An experiment using changes in the absorbance of tyrosine residues in CaM to probe melting observed processes on hundreds of microsecond time scales. As explained above, however, on the basis of this new information these are most likely to be assignable to the activated barrier crossing processes such as those reported for ubiquitin.[11] Thus, by probing the fastest steps in CaM domain melting, our new results complement this prior study to produce an overall picture of CaM domain melting. Taken jointly, these two studies also reinforce the need to observe protein dynamics over as wide a range of time scales as possible to gain a complete molecular picture.

ASSOCIATED CONTENT

Supporting Information

The Supporting Information is available free of charge on the ACS Publications website at DOI: 10.1021/acs.jpcb.9b08870.

Details of materials and methods, including calibration of the T-jump spectrometer and additional fitting of dynamic data (PDF)

AUTHOR INFORMATION

Corresponding Author

*E-mail: neil.hunt@york.ac.uk.

ORCID

Daniel J. Shaw: 0000-0003-0090-2947

Neil T. Hunt: 0000-0001-7400-5152

Notes

The authors declare no competing financial interest.

DOI: 10.1021/acs.jpcb.9b08870
J. Phys. Chem. B XXXX, XXX, XXX−XXX

■ ACKNOWLEDGMENTS

Funding from STFC is gratefully acknowledged for program access to the Central Laser Facility ULTRA spectrometer. L.M. gratefully acknowledges studentship support from STFC Central Laser Facility and the University of Strathclyde. R.F. gratefully acknowledges studentship support from the University of Strathclyde.

■ REFERENCES

(1) Gilmanshin, R.; Williams, S.; Callender, R. H.; Woodruff, W. H.; Dyer, R. B. Fast events in protein folding: Relaxation dynamics of secondary and tertiary structure in native apomyoglobin. *Proc. Natl. Acad. Sci. U. S. A.* **1997**, *94*, 3709.

(2) Petty, S. A.; Volk, M. Fast folding dynamics of an alpha-helical peptide with bulky side chains. *Phys. Chem. Chem. Phys.* **2004**, *6*, 1022−1030.

(3) Williams, S.; Causgrove, T. P.; Gilmanshin, R.; Fang, K. S.; Callender, R. H.; Woodruff, W. H.; Dyer, R. B. Fast events in protein folding: Helix melting and formation in a small peptide. *Biochemistry* **1996**, *35*, 691−697.

(4) Chung, H. S.; Khalil, M.; Smith, A. W.; Tokmakoff, A. Transient two-dimensional IR spectrometer for probing nanosecond temperature-jump kinetics. *Rev. Sci. Instrum.* **2007**, *78*, No. 063101.

(5) Rigler, R.; Rabl, C. R.; Jovin, T. M. Temperature-jump apparatus for fluorescence measurements. *Rev. Sci. Instrum.* **1974**, *45*, 580−588.

(6) Khuc, M. T.; Mendonca, L.; Sharma, S.; Solinas, X.; Volk, M.; Hache, F. Measurement of circular dichroism dynamics in a nanosecond temperature-jump experiment. *Rev. Sci. Instrum.* **2011**, *82*, No. 054302.

(7) Sanstead, P. J.; Tokmakoff, A. Direct observation of activated kinetics and downhill dynamics in DNA dehybridization. *J. Phys. Chem. B* **2018**, *122*, 3088−3100.

(8) Zhang, X. X.; Jones, K. C.; Fitzpatrick, A.; Peng, C. S.; Feng, C. J.; Baiz, C. R.; Tokmakoff, A. Studying Protein-Protein Binding through T-Jump Induced Dissociation: Transient 2D IR Spectroscopy of Insulin Dimer. *J. Phys. Chem. B* **2016**, *120*, 5134−5145.

(9) Sanstead, P. J.; Stevenson, P.; Tokmakoff, A. Sequence-dependent mechanism of DNA oligonucleotide dehybridization resolved through infrared spectroscopy. *J. Am. Chem. Soc.* **2016**, *138*, 11792−11801.

(10) Jones, K. C.; Peng, C. S.; Tokmakoff, A. Folding of a heterogeneous beta-hairpin peptide from temperature-jump 2D IR spectroscopy. *Proc. Natl. Acad. Sci. U. S. A.* **2013**, *110*, 2828−2833.

(11) Chung, H. S.; Tokmakoff, A. Temperature-dependent downhill unfolding of ubiquitin. I. Nanosecond-to-millisecond resolved nonlinear infrared spectroscopy. *Proteins: Struct., Funct., Genet.* **2008**, *72*, 474−487.

(12) Smith, A. W.; Tokmakoff, A. Probing local structural events in beta-hairpin unfolding with transient nonlinear infrared spectroscopy. *Angew. Chem., Int. Ed.* **2007**, *46*, 7984−7987.

(13) Chung, H. S.; Ganim, Z.; Jones, K. C.; Tokmakoff, A. Transient 2D IR spectroscopy of ubiquitin unfolding dynamics. *Proc. Natl. Acad. Sci. U. S. A.* **2007**, *104*, 14237−14242.

(14) Scheerer, D.; Chi, H.; McElheny, D.; Keiderling, T. A.; Hauser, K. Isotopically site-selected dynamics of a three-stranded beta-sheet peptide detected with temperature-jump infrared-spectroscopy. *J. Phys. Chem. B* **2018**, *122*, 10445−10454.

(15) Popp, A.; Scheerer, D.; Heck, B.; Hauser, K. Biomolecular dynamics studied with IR-spectroscopy using quantum cascade lasers combined with nanosecond perturbation techniques. *Spectrochim. Acta, Part A* **2017**, *181*, 192−199.

(16) Krejtschi, C.; Hauser, K. Stability and folding dynamics of polyglutamic acid. *Eur. Biophys. J.* **2011**, *40*, 673−685.

(17) Phillips, C. M.; Mizutani, Y.; Hochstrasser, R. M. Ultrafast thermally-induced unfolding of RNAse-A. *Proc. Natl. Acad. Sci. U. S. A.* **1995**, *92*, 7292−7296.

(18) Donten, M. L.; Hassan, S.; Popp, A.; Halter, J.; Hauser, K.; Hamm, P. pH-jump induced leucine zipper folding beyond the diffusion limit. *J. Phys. Chem. B* **2015**, *119*, 1425−1432.

(19) Deeg, A. A.; Rampp, M. S.; Popp, A.; Pilles, B. M.; Schrader, T. E.; Moroder, L.; Hauser, K.; Zinth, W. Isomerization- and temperature-jump-induced dynamics of a photoswitchable beta-hairpin. *Chem. - Eur. J.* **2014**, *20*, 694−703.

(20) Backus, E. H. G.; Bloem, R.; Donaldson, P. M.; Ihalainen, J. A.; Pfister, R.; Paoli, B.; Caflisch, A.; Hamm, P. 2D-IR study of a photoswitchable isotope-labeled alpha-helix. *J. Phys. Chem. B* **2010**, *114*, 3735−3740.

(21) Hamm, P.; Helbing, J.; Bredenbeck, J. Two-dimensional infrared spectroscopy of photoswitchable peptides. *Annu. Rev. Phys. Chem.* **2008**, *59*, 291−317.

(22) Kolano, C.; Helbing, J.; Kozinski, M.; Sander, W.; Hamm, P. Watching hydrogen-bond dynamics in a beta-turn by transient two-dimensional infrared spectroscopy. *Nature* **2006**, *444*, 469−472.

(23) Jones, K. C.; Peng, C. S.; Tokmakoff, A. Folding of a heterogeneous β-hairpin peptide from temperature-jump 2D IR spectroscopy. *Proc. Natl. Acad. Sci. U. S. A.* **2013**, *110*, 2828−2833.

(24) Chung, H. S.; Tokmakoff, A. Temperature-dependent downhill unfolding of ubiquitin. II. Modeling the free energy surface. *Proteins: Struct., Funct., Genet.* **2008**, *72*, 488−497.

(25) Fritzsch, R.; Greetham, G. M.; Clark, I. P.; Minnes, L.; Towrie, M.; Parker, A. W.; Hunt, N. T. Monitoring base-specific dynamics during melting of DNA−ligand complexes using temperature-jump time-resolved infrared spectroscopy. *J. Phys. Chem. B* **2019**, *123*, 6188−6199.

(26) Park, H. Y.; Kim, S. A.; Korlach, J.; Rhoades, E.; Kwok, L. W.; Zipfel, W. R.; Waxham, M. N.; Webb, W. W.; Pollack, L. Conformational changes of calmodulin upon Ca^{2+} binding studied with a microfluidic mixer. *Proc. Natl. Acad. Sci. U. S. A.* **2008**, *105*, 542−547.

(27) Trewhella, J.; Liddle, W. K.; Heidorn, D. B.; Strynadka, N. Calmodulin and troponin-c structures studied by fourier-transform infrared-spectroscopy - effects of Ca^{2+} and Mg^{2+} binding. *Biochemistry* **1989**, *28*, 1294−1301.

(28) Rainteau, D.; Wolf, C.; Lavialle, F. Effects of calcium and calcium analogs on calmodulin - a Fourier-transform infrared and electron-spin resonance investigation. *Biochim. Biophys. Acta, Mol. Cell Res.* **1989**, *1011*, 81−87.

(29) Matsushima, N.; Izumi, Y.; Matsuo, T.; Yoshino, H.; Ueki, T.; Miyake, Y. Binding of both Ca^{2+} and mastoparan to calmodulin induces a large change in the tertiary structure. *J. Biochem.* **1989**, *105*, 883−887.

(30) Linse, S.; Helmersson, A.; Forsen, S. Calcium-binding to calmodulin and its globular domains. *J. Biol. Chem.* **1991**, *266*, 8050−8054.

(31) Zhang, M.; Tanaka, T.; Ikura, M. Calcium-induced conformational transition revealed by the solution structure of apo calmodulin. *Nat. Struct. Mol. Biol.* **1995**, *2*, 758−767.

(32) Kleinjung, J.; Fraternali, F.; Martin, S. R.; Bayley, P. M. Thermal unfolding simulations of apo-calmodulin using leap-dynamics. *Proteins: Struct., Funct., Genet.* **2003**, *50*, 648−656.

(33) Jones, E. M.; Balakrishnan, G.; Squier, T. C.; Spiro, T. G. Distinguishing unfolding and functional conformational transitions of calmodulin using ultraviolet resonance Raman spectroscopy. *Protein Sci.* **2014**, *23*, 1094−1101.

(34) Yamniuk, A. P.; Ishida, H.; Lippert, D.; Vogel, H. J. Thermodynamic Effects of Noncoded and Coded Methionine Substitutions in Calmodulin. *Biophys. J.* **2009**, *96*, 1495−1507.

(35) Rabl, C. R.; Martin, S. R.; Neumann, E.; Bayley, P. M. Temperature jump kinetic study of the stability of apo-calmodulin. *Biophys. Chem.* **2002**, *101*, 553−564.

(36) Masino, L.; Martin, S. R.; Bayley, P. M. Ligand binding and thermodynamic stability of a multidomain protein, calmodulin. *Protein Sci.* **2000**, *9*, 1519−1529.

(37) Browne, J. P.; Strom, M.; Martin, S. R.; Bayley, P. M. The role of beta-sheet interactions in domain stability, folding, and target recognition reactions of calmodulin. *Biochemistry* **1997**, *36*, 9550−9561.

(38) Barbato, G.; Ikura, M.; Kay, L. E.; Pastor, R. W.; Bax, A. Backbone dynamics of calmodulin studied by ^{15}N relaxation using inverse

DOI: 10.1021/acs.jpcb.9b08870
J. Phys. Chem. B XXXX, XXX, XXX−XXX

detected 2-dimensional NMR-spectroscopy - the central helix is flexible. *Biochemistry* **1992**, *31*, 5269−5278.
(39) Ikura, M.; Spera, S.; Barbato, G.; Kay, L. E.; Krinks, M.; Bax, A. Secondary structure and side-chain ^{1}H and ^{13}C resonance assignments of calmodulin in solution by heteronuclear multidimensional NMR-spectroscopy. *Biochemistry* **1991**, *30*, 9216−9228.
(40) Heidorn, D. B.; Trewhella, J. Comparison of the crystal and solution structures of calmodulin and troponin-C. *Biochemistry* **1988**, *27*, 909−915.
(41) Seaton, B. A.; Head, J. F.; Engelman, D. M.; Richards, F. M. Calcium-induced increase in the radius of gyration and maximum dimension of calmodulin measured by small-angle x-ray-scattering. *Biochemistry* **1985**, *24*, 6740−6743.
(42) Seaton, B. A.; Head, J. F.; Lord, R. C.; Petsko, G. A. Studies of calmodulin structure - laser raman-spectroscopy of biomolecules. *Biochemistry* **1983**, *22*, 973−978.
(43) Guerini, D.; Krebs, J. Influence of temperature and denaturing agents on the structural stability of calmodulin - a ^{1}H nuclear magnetic-resonance study. *FEBS Lett.* **1983**, *164*, 105−110.
(44) Brzeska, H.; Venyaminov, S. V.; Grabarek, Z.; Drabikowski, W. Comparative studies on thermostability of calmodulin, skeletal-muscle troponin-c and their tryptic fragments. *FEBS Lett.* **1983**, *153*, 169−173.
(45) Stigler, J.; Rief, M. Calcium-dependent folding of single calmodulin molecules. *Proc. Natl. Acad. Sci. U. S. A.* **2012**, *109*, 17814−17819.
(46) Tripathi, S.; Portman, J. J. Inherent flexibility determines the transition mechanisms of the EF-hands of calmodulin. *Proc. Natl. Acad. Sci. U. S. A.* **2009**, *106*, 2104−2109.
(47) Zhu, M. M.; Rempel, D. L.; Zhao, J.; Giblin, D. E.; Gross, M. L. Probing Ca2+-induced conformational changes in porcine calmodulin by H/D exchange and ESI-MS: Effect of cations and ionic strength. *Biochemistry* **2003**, *42*, 15388−15397.
(48) Sorensen, B. R.; Shea, M. A. Calcium binding decreases the Stokes radius of calmodulin and mutants R74A, R90A, and R90G. *Biophys. J.* **1996**, *71*, 3407−3420.
(49) Swulius, M. T.; Waxham, M. N. Ca^{2+}/calmodulin-dependent protein kinases. *Cell. Mol. Life Sci.* **2008**, *65*, 2637−2657.
(50) Su, Z. Z.; Blazing, M. A.; Fan, D.; George, S. E. The calmodulin-nitric oxide synthase interaction - critical role of the calmodulin latch domain in enzyme activation. *J. Biol. Chem.* **1995**, *270*, 29117−29122.
(51) Wolf, B. A.; Colca, J. R.; McDaniel, M. L. Calmodulin inhibits inositol trisphosphate-induced ca-2+ mobilization from the endoplasmic-reticulum of islets. *Biochem. Biophys. Res. Commun.* **1986**, *141*, 418−425.
(52) Tanokura, M.; Yamada, K. Effects of trifluoperazine on calcium-binding by calmodulin - heat-capacity and entropy changes. *J. Biol. Chem.* **1986**, *261*, 749−752.
(53) Andreasen, T. J.; Luetje, C. W.; Heideman, W.; Storm, D. R. Purification of a novel calmodulin binding-protein from bovine cerebral-cortex membranes. *Biochemistry* **1983**, *22*, 4615−4618.
(54) Minnes, L.; Shaw, D. J.; Cossins, B.; Donaldson, P. M.; Greetham, G. M.; Towrie, M.; Parker, A. W.; Baker, M. J.; Henry, A.; Taylor, R.; et al. Quantifying secondary structure changes in calmodulin using 2D-IR spectroscopy. *Anal. Chem.* **2017**, *89*, 10898−10906.

DOI: 10.1021/acs.jpcb.9b08870
J. Phys. Chem. B XXXX, XXX, XXX−XXX